Double differential cross sections of light charged particle production for the n+^{238}U reaction *

Hai-Rui Guo(郭海瑞)[1] Yin-Lu Han(韩银录)[2;1)] Chong-Hai Cai(蔡崇海)[3]

[1] Institute of Applied Physics and Computational Mathematics, Beijing 100094, China
[2] China Institute of Atomic Energy, P.O. Box 275(41), Beijing 102413, China
[3] Department of Physics, Nankai University, Tianjin 300071, China

Abstract: Production of light complex particles from the n+^{238}U reaction is analyzed with the exciton model including the improved Iwamoto-Harada pickup mechanism for the preequilibrium process. It is allowed that some of the nucleons forming the complex ejectile come from levels below the Fermi energy, and the intrinsic structure of the emitted particle is taken into account. The equilibrium-state emissions are also considered by using Hauser-Feshbach theory with the width fluctuation correction and the evaporation model. Moreover, all cross sections, angular distributions, energy spectra and double differential cross sections of neutron, proton, deuteron, triton and alpha emissions for the n+^{238}U reaction are consistently calculated and analyzed with nuclear theoretical models in the energy range $E_{\rm n}\leqslant 150$ MeV. ENDF-formatted nuclear data including information about the production of light charged particles are obtained.

Keywords: light charged particle production, nuclear reaction theoretical model, n+^{238}U reaction, nuclear data at $E_{\rm n}\leqslant 150$ MeV

PACS: 25.85.Ec, 24.60.Dr, 25.40.-h **DOI:** 10.1088/1674-1137/42/12/124101

1 Introduction

Since ^{238}U is usually the major component of nuclear fuel and nuclear waste, the analysis of neutron-induced reactions on ^{238}U at incident energies below 150 MeV is of great importance in the field of nuclear energy and nuclear waste transmutation [1, 2], including for the design of accelerator driven systems (ADS). In such reactions, the light charged particle (proton, deuteron, triton and alpha) production is almost negligible at incident energies below 20 MeV, while their contribution becomes larger as the incident energy increases. Data on light charged particle (LCP) production are as important as those on neutron production for ADS [3], as they are required in the calculation of heat. However, no evaluation data exist which include LCP production, and the theoretical prediction of LCP production is a challenging problem.

A set of experimental data on double differential cross sections (DDXs) and energy spectra of LCP emission from neutron-induced reactions on natural uranium at several incident energies from 25 to 65 MeV was measured [4]. Later, another set of DDXs of LCP production induced by 96 MeV neutrons on natural uranium was available [5]. These two sets of experimental data are currently the only measurements of DDX of LCP production for neutron-induced reactions on actinides. They provide a requisite base to test nuclear theoretical models for LCP production predictions and comprehensive analysis of neutron-induced reactions on actinides at intermediate energies. Raeymackers et al. [4] and Blideanu et al. [5] used three different approaches to predict these DDXs. The first was the original exciton model [6] embodied in the GNASH code [7]. In the exciton model, complex particle emission is treated by an arrangement factor [8]. The calculated results strongly underestimated the experimental data for complex particle production. The second was the Kalbach semi-empirical method [9, 10] adopted in the TALYS code [11]. It is well known that for neutron-induced complex-particle emission reactions, directlike mechanisms such as pickup are important and not entirely included by the original exciton model. The Kalbach semi-empirical method considers the directlike mechanisms using systematics and combines them with the original exciton model. Some improvements were obtained using the Kalbach semi-empirical method compared to the original exciton model, but there was still considerable underestimation.

Received 10 July 2018, Published online 29 October 2018

∗ Supported by National Natural Science Foundation of China-NSAF (U1630122), IAEA Coordinated Research Projects (CRPs) on Recommended Input Parameter Library (RIPL) for Fission Cross Section Calculations (20464) and Science Challenge Project (TZ2018005)

1) E-mail: hanyl@ciae.ac.cn

The third was the approach proposed by Ribanský and Obložinský [12], which assumes that complex ejectiles are formed from excited nucleons within the same volume in momentum space during the preequilibrium process. The third approach obtained a better agreement, but its predictive power is limited because it contains some cluster formation probabilities γ_β which are free parameters and determined by fitting the experimental data.

A microscopic DYWAN model [13] was also proposed for the theoretical description of neutron-induced reactions at intermediate energies. This model treated the nuclear dynamics using the wavelet technique. However, the model greatly overestimates the LCP production.

In this paper, we use the exciton model with an improved Iwamoto-Harada pickup mechanism [14–16] to analyze the LCP production. The theoretical model was originally proposed by Iwamoto and Harada [14], and improved by Zhang et al. by considering the restriction of the excitation energy [15, 16]. The main physical idea is that some of the nucleons forming the complex ejectiles can come from the levels below the Fermi surface, and the formation probability of the complex particle is calculated explicitly with the statistical phase space integration method. The details of the model will be described in Section 2. The equilibrium-state contribution is also analyzed with Hauser-Feshbach theory with the width fluctuation correction and the evaporation model. Since the available experimental data on LCP production from neutron-induced reactions on uranium are scarce, consistent calculation of all the channels of the n+^{238}U reaction is required in order to predict the LCP production cross sections reliably. Therefore, the purpose of this paper is to test the reliability of the exciton model considering the improved Iwamoto-Harada pickup mechanism used to predict the complex particle production induced by neutrons on fission nuclei, and to calculate the physical quantities of all reaction channels of the n+^{238}U reaction and give ENDF-formatted nuclear data in the incident energy region $E_{\rm n}\leqslant$150 MeV.

Section 2 gives a brief description of the theoretical models applied in this work. Section 3 compares the calculated results with experimental data and analyses. Section 4 gives our conclusion.

2 Theoretical models

The optical model is applied to predict the total, nonelastic, and elastic scattering cross sections, and the elastic scattering angular distribution, as well as to calculate the transmission coefficients and inverse cross sections of compound-process particle emission. The neutron and proton optical model potentials are taken from Ref. [17]. The deuteron [18], triton [19] and alpha particle [20] optical model potentials are adopted in the statistical model calculation. The direct inelastic scattering cross sections and angular distributions are analyzed by using the distorted wave Born approximation (DWBA) theory.

The equilibrium and preequilibrium emission processes are analyzed by using the unified Hauser-Feshbach and exciton model [15] at incident energies below 20 MeV, and by using the Hauser-Feshbach theory with width fluctuation correction, evaporation model, intranuclear cascade model and exciton model above 20 MeV. The exciton model assumes that the incident nucleon and the target nucleus interact through the nucleon-nucleon interaction and form a compound system excited to a particle-hole (p-h) state. Then successive nucleon-nucleon interactions in the compound system lead the system to exciton states with higher exciton number, and eventually result in a fully equilibrium state. In the process, nucleons or clusters of nucleons can be excited occasionally to unbound states and subsequently be emitted. In the framework of the exciton model, the improved Iwamoto-Harada model is applied to describe the complex particle emission in the preequilibrium process. This model allows that some of the nucleons forming the complex ejectiles can come from levels below the Fermi energy, and introduces the probability of several nucleons forming the complex particle, so the pickup type contribution of the composite particle emission is considered in this model. The internal structure of the emitted complex particle is taken into account in the formation probability. In this work, the internal structure of the emitted particle is described with a harmonic oscillator wave function. The formation probability is assumed to be proportional to the number of the microscopic states occupied by the complex particle in the phase space and calculated explicitly with the Fermi-gas model, namely,

$$F^b_{lm}(E^*,\varepsilon)=\frac{1}{(2\pi\hbar)^{3(N-1)}}\int\prod_{i=1}^{N-1}{\rm d}\boldsymbol{p}_i{\rm d}\boldsymbol{r}_i, \tag{1}$$

where $F^b_{lm}(E^*,\varepsilon)$ is the formation probability of particle b with l nucleons above the Fermi level and m nucleons below. E^* is the excitation energy of the compound system. ε is the outgoing energy. N is the nucleon number of the b particle, and $\boldsymbol{r}_i$ and $\boldsymbol{p}_i$ are the intrinsic relative coordinates and momenta of the b particle.

The emission rate of the b particle in the exciton state n is obtained by

$$\begin{aligned}W^{J\pi}_b(n,E^*,\varepsilon) =& \frac{2s_b+1}{\pi^2\hbar^3}\mu_b\sigma^{J\pi}_b(\varepsilon)\varepsilon F^b_{lm}(E^*,\varepsilon)Q_b(n)\\ &\times\frac{\omega(p-1,h,E^*-\varepsilon-B_b)}{\omega(p,h,E^*)},\end{aligned} \tag{2}$$

where s_b, μ_b, B_b, $\sigma^{J\pi}_b$ denote the spin, reduced mass, binding energy and inverse cross section, respectively, of the b particle. $F^b_{lm}(E^*,\varepsilon)$=1 for nucleons. $Q_b(n)$ is the

combination factor, which gives the combination probability of the emitted particle at the exciton state n and the effect of the projectile type. $\omega(p,h,E^*)$ denotes the exciton state density. The expressions for $Q_b(n)$ and $\omega(p,h,E^*)$ are given in Refs. [15, 16].

Fission is included as a decay channel of equilibrium states. The Bohr-Wheeler theory [21, 22] is applied in the transmission coefficient calculation at each fission barrier. The fission spectrum is calculated by an energy-dependent Watt spectrum.

The angular dependent formula of Kalbach systematics [23, 24] is used to obtain the DDXs of neutron, proton, deuteron, triton and alpha emissions on the base of the calculated energy spectra.

3 Calculated results and analysis

The total, non-elastic and elastic scattering cross sections, and elastic scattering angular distribution, are calculated by using the global optical model potential [17]. The inelastic scattering cross sections and angular distributions are calculated with DWBA and nuclear reaction statistical theories. The calculated results are in good agreement with experimental data, as shown in Ref. [17].

The calculated results of fission, (n, xn) and (n, γ) cross sections also reproduce the experimental data well. The calculated fission cross section is compared with the experimental data [25–27] in Fig. 1. The crosses denote a set of new experimental data [25] which was measured at the Los Alamos Neutron Science Center (LANSCE) with world-class advanced experimental facilities in 2014, after the release of ENDF/B-VII.1 and JENDL-4.0. The new experimental data are consistent with the previous data taken from Ref. [26] and denoted by the solid squares. The calculated result is in good agreement with the experimental data taken from Refs. [25, 26], and similar to the data from ENDF/B-VII.1 (dashed lines) at incident energies below 30 MeV. The JENDL-4.0 data (long-dashed lines) are lower than the experimental data at some energies.

Based on the agreement of all calculated cross sections and angular distributions with experimental data, the energy spectra and DDXs for neutron, proton, deuteron, triton and alpha emissions, and the γ production energy spectrum, are calculated with the theoretical models.

The calculated proton emission energy spectra at incident neutron energies from 25.5 to 62.7 MeV are compared with experimental data [4] in Fig. 2. The calculated results at incident energies above 37.5 MeV are in good agreement with experimental data. The shape of the calculated result curves at incident energies below 37.5 MeV is consistent with that of experimental data, but the magnitude is smaller. The calculated results are smaller than experimental data at lower emission energies, where the contribution is mainly from the equilibrium reaction and suppressed by the Coulomb barrier.

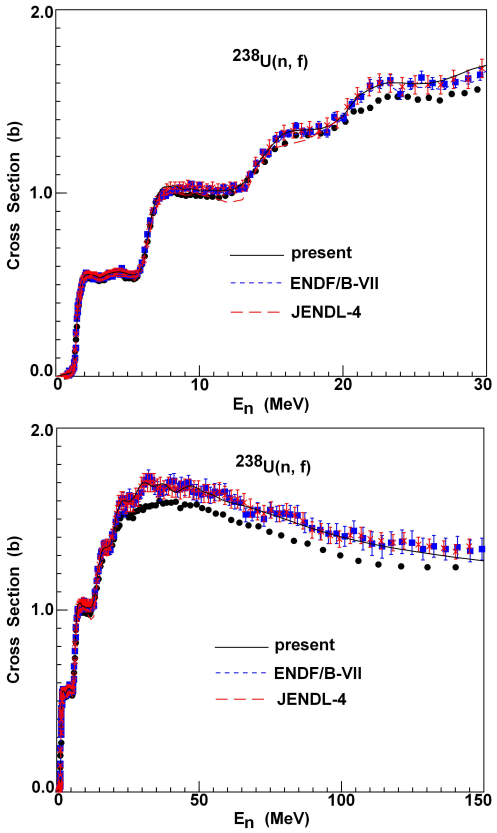

Fig. 1. (color online) Calculated results for fission cross section (solid lines) compared with the experimental data (crosses [25], solid squares [26], and solid circles [27]) and the evaluated data from ENDF/B-VII.1 (dashed lines) and JENDL-4.0 (long-dashed lines) at incident energies below 30 MeV and below 150 MeV.

The calculated deuteron emission energy spectra at incident neutron energies from 28.5 to 62.7 MeV are compared with experimental data [4] in Fig. 3. The calculated results are in reasonable agreement with experimental data at incident energies below 49 MeV and smaller than experimental data above 53.5 MeV.

The calculated triton emission energy spectra are compared with experimental data at incident energies from 41.0 to 62.7 MeV in Fig. 4. The calculated results reproduce the experimental data well except that the calculated results at incident energies of 41.0, 45.0 and 49.0 MeV are larger than experimental data in the middle emission energy region.

The calculated alpha emission energy spectra are compared with experimental data at incident energies from 34.5 to 62.7 MeV in Fig. 5. The calculated results are in good agreement with experimental data for emission energy above 25.0 MeV. It can be seen that the

emission probability decreases with increasing emission energy. The calculated results are smaller than experimental data at emission energies below about 25.0 MeV, where the equilibrium emission is dominant.

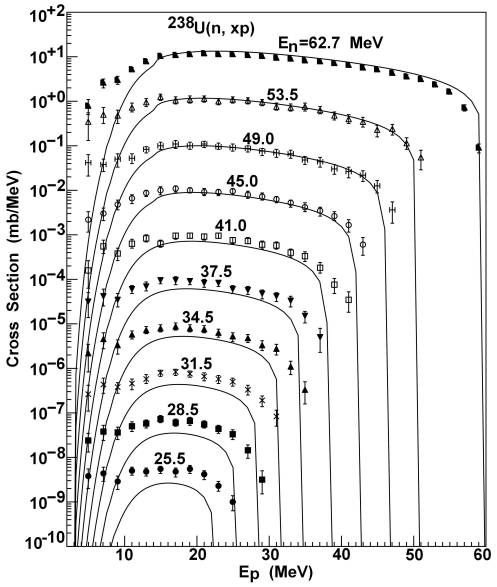

Fig. 2. Calculated proton emission spectra compared with experimental data [4]. The data are shifted downward by factors of 10^0, 10^{-1}, 10^{-2}, etc.

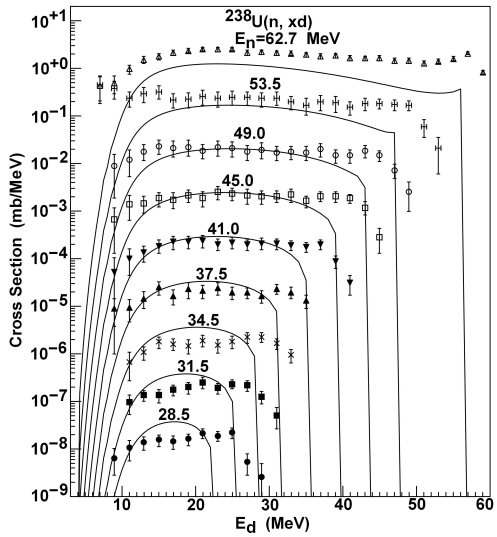

Fig. 3. Calculated deuteron emission spectra compared with experimental data [4]. The data are shifted downward by factors of 10^0, 10^{-1}, 10^{-2}, etc.

The proton emission DDXs are compared with experimental data at incident neutron energies from 25.5 to 62.7 MeV. The calculated results at incident neutron energies 25.5, 28.5, 31.5, 34.5 and 37.5 MeV are in good agreement with experimental data for proton emission angles above 90.0° and emission energies above 10.0 MeV. The shapes of the calculated result curves for proton emission angles below 90° are in good agreement with those of experimental data, but the magnitude is smaller at these incident energies. A comparison of calculated results with experimental data at incident energy 34.5 MeV is given in Fig. 6. The calculated results at incident energies from 41.0 to 62.7 MeV are in good agreement with experimental data. Figure 7 shows the comparison at incident energy of 45.0 MeV. The proton emission DDXs at incident energy of 96.0 MeV are compared with experimental data [5] in Fig. 8. A reasonable agreement is obtained.

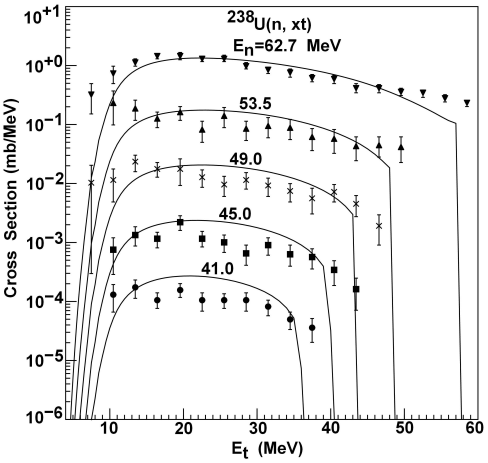

Fig. 4. Calculated triton emission spectra compared with experimental data [4]. The data are shifted downward by factors of 10^0, 10^{-1}, 10^{-2}, etc.

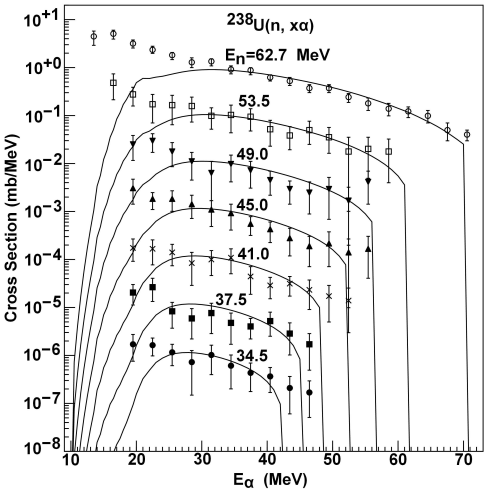

Fig. 5. Calculated alpha emission spectra compared with experimental data [4]. The data are shifted downward by factors of 10^0, 10^{-1}, 10^{-2}, etc.

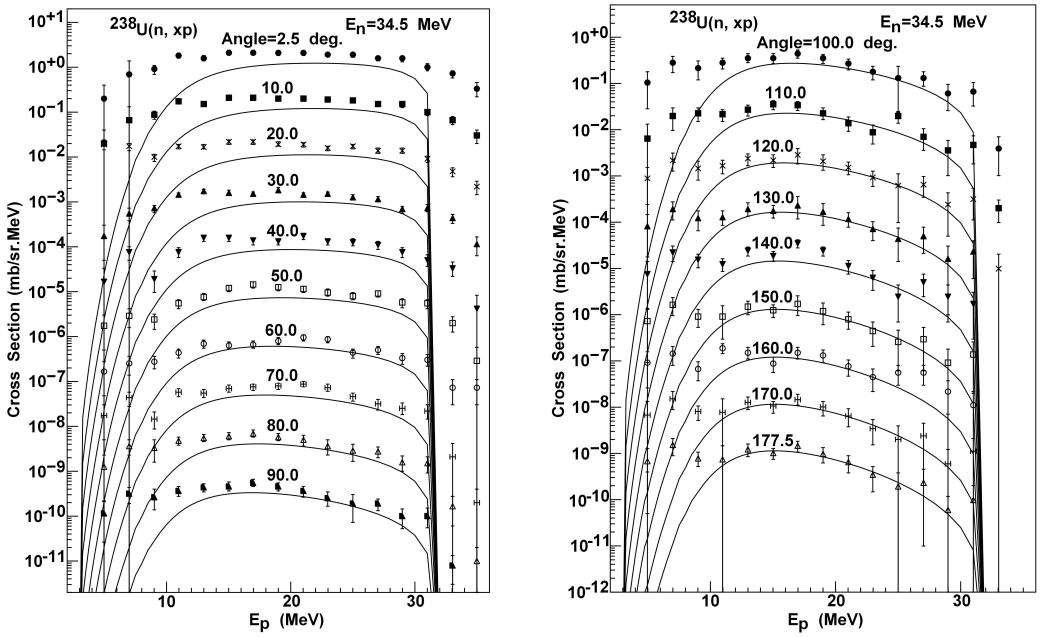

Fig. 6. Calculated proton emission DDXs compared with experimental data [4] at incident energy of 34.5 MeV. The data are shifted downward by factors of 10^0, 10^{-1}, 10^{-2}, etc.

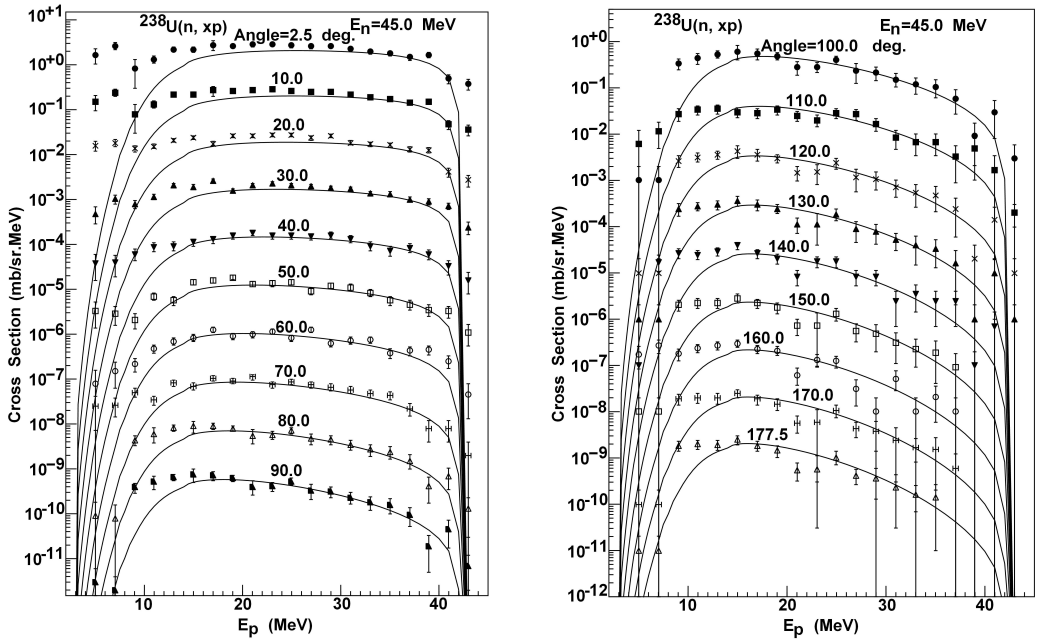

Fig. 7. Calculated proton emission DDXs compared with experimental data [4] at incident energy of 45.0 MeV. The data are shifted downward by factors of 10^0, 10^{-1}, 10^{-2}, etc.

The calculated deuteron emission DDXs are compared with experimental data [4, 5] at incident energies from 28.5 to 96 MeV. The calculated results are in reasonable agreement with experimental data at incident energies below 49.0 MeV. Figure 9 shows the comparison of calculated results with experimental data at incident energy of 45.0 MeV. The calculated results at incident energies 53.5, 62.7 and 96.0 MeV are consistent with experimental data for emission angles above 50.0°, but lower than experimental data below 50.0°, especially for the higher emission energy region. The comparison of calculated results with experimental data at incident energy of 53.5 MeV is given in Fig. 10. The underestimation for the higher emission energy region may be

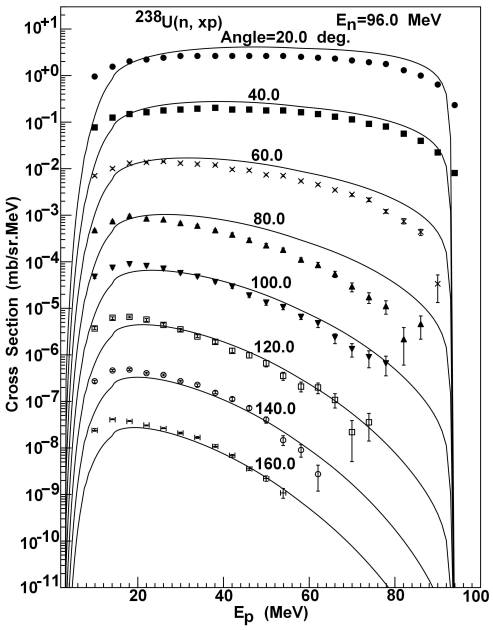

Fig. 8. Calculated proton emission DDXs compared with experimental data [4] at incident energy of 96.0 MeV. The data are shifted downward by factors of 10^0, 10^{-1}, 10^{-2}, etc. The experimental data are taken from Ref. [5]

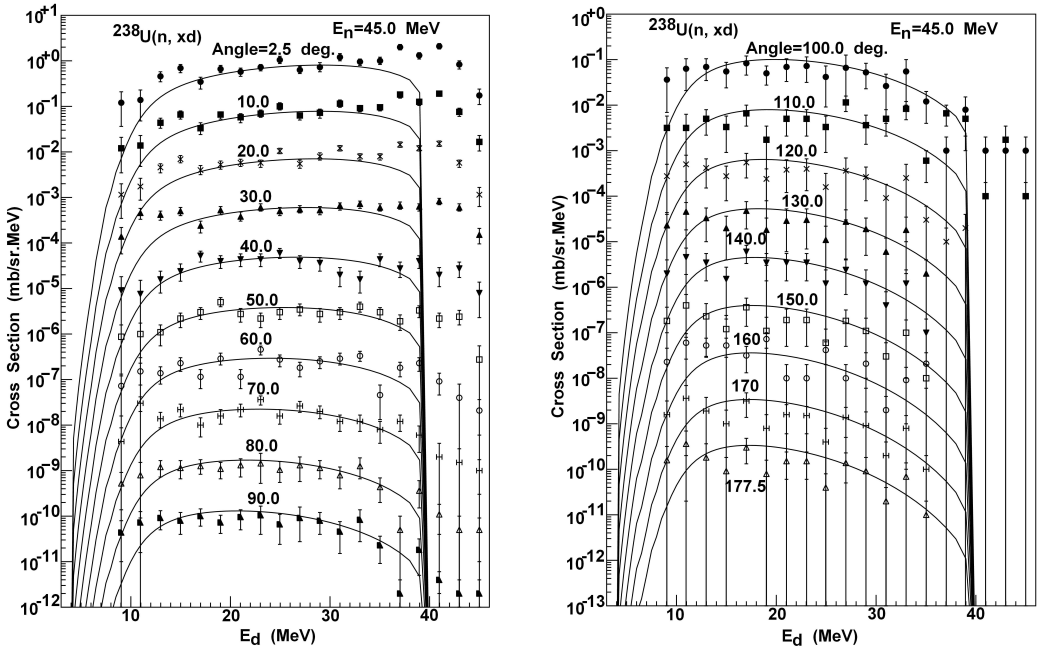

Fig. 9. Calculated deuteron emission DDXs compared with experimental data [4] at incident energy 45.0 MeV. The data are shifted downward by factors of 10^0, 10^{-1}, 10^{-2}, etc.

because the contributions of direct (n, xd) reactions, such as the knock-out reaction, are not considered. Accordingly, the energy spectra at incident energies of 53.5 and 62.7 MeV are also underestimated, as shown in Fig. 3.

The triton emission DDXs are compared with experimental data at incident energies 41.0, 45.0, 49.0, 53.5 and 62.7 MeV. The calculated results at incident energies below 53.5 MeV are in reasonable agreement with experimental data except for some emission angles. For those emission angles, the experimental data have some big structures which are not physically reasonable. The comparisons of calculated results with experimental data at incident energies of 49.0 and 53.5 MeV are given in Figs. 11 and 12. Some structures in the experimental

data can be seen for angles of 30° and 40° at incident energy of 49 MeV and for angles above 90° at incident energy of 53.5 MeV. The calculated results at incident energy of 62.7 MeV are in good agreement with experimental data, as shown in Fig. 13. The shapes of the calculated result curves at incident energy of 96.0 MeV are in good agreement with those of experimental data, as shown in Fig. 14, while the magnitudes of the calculated results are smaller. Since the calculated results for triton emission DDXs are larger than experimental data for some emission angles at incident neutron energies below 53.5 MeV, the calculated results for the energy spectra are correspondingly larger than experimental data, as shown in Fig. 4.

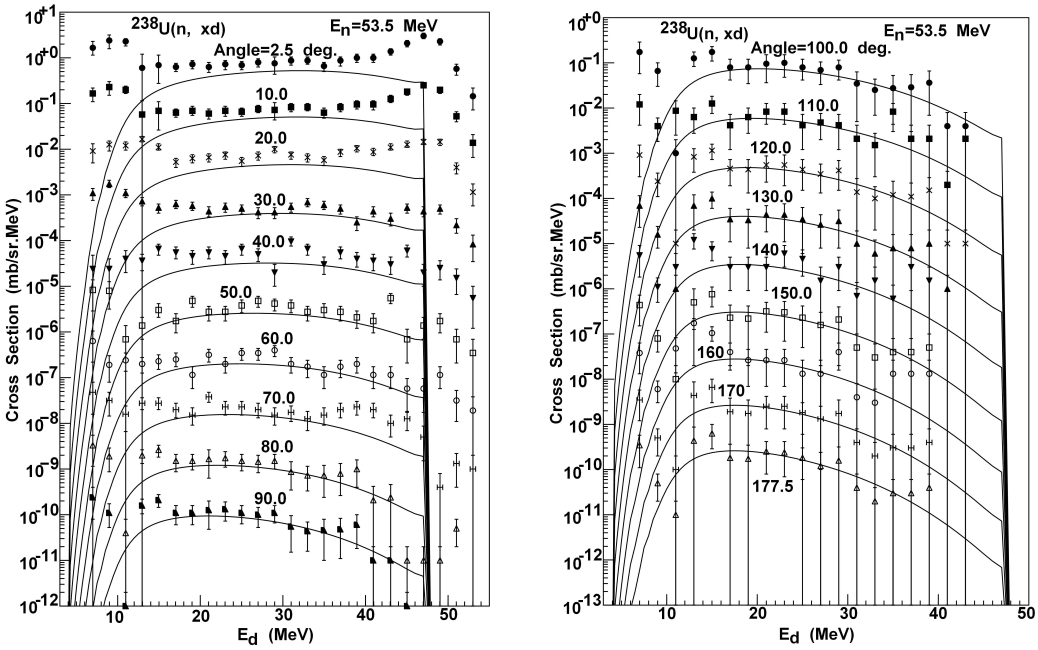

Fig. 10. Calculated deuteron emission DDXs compared with experimental data [4] at incident energy 53.5 MeV. The data are shifted downward by factors of 10^0, 10^{-1}, 10^{-2}, etc.

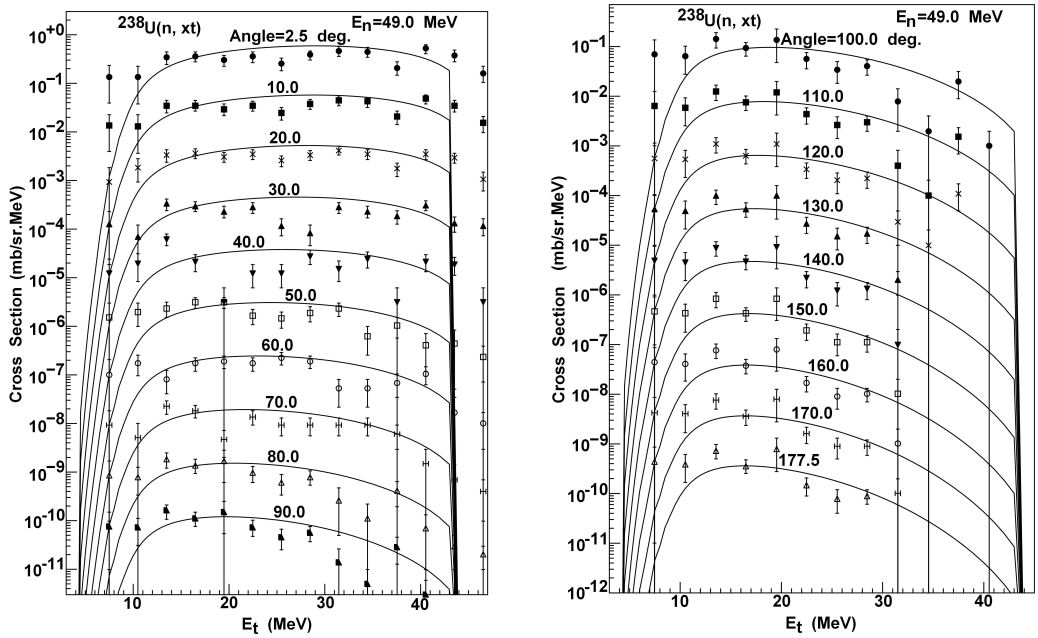

Fig. 11. Calculated triton emission DDXs compared with experimental data [4] at incident energy 49.0 MeV. The data are shifted downward by factors of 10^0, 10^{-1}, 10^{-2}, etc.

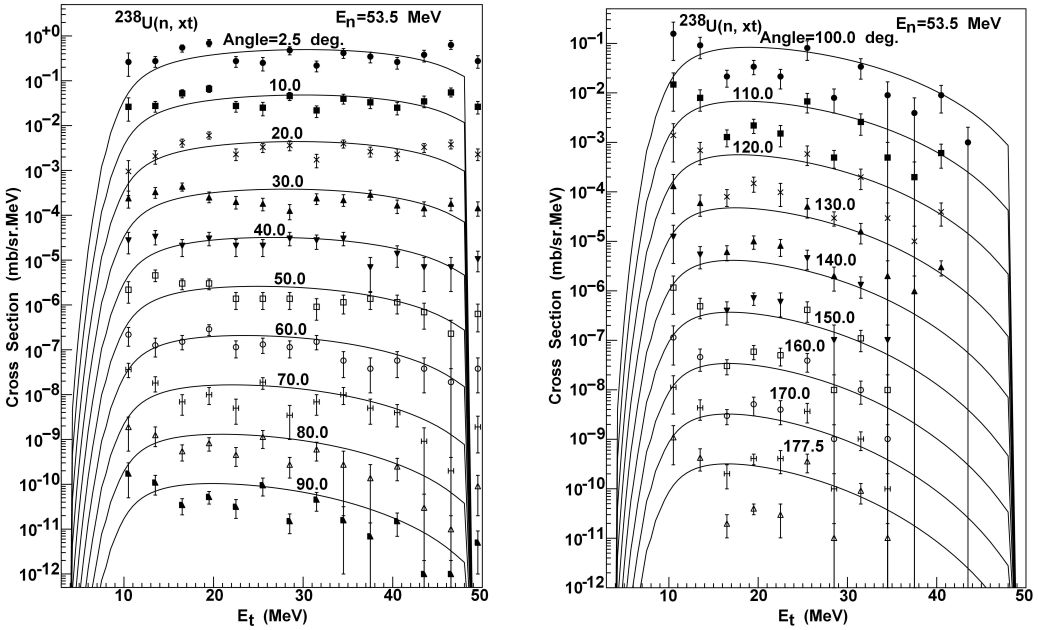

Fig. 12. Calculated triton emission DDXs compared with experimental data [4] at incident energy 53.5 MeV. The data are shifted downward by factors of 10^0, 10^{-1}, 10^{-2}, etc.

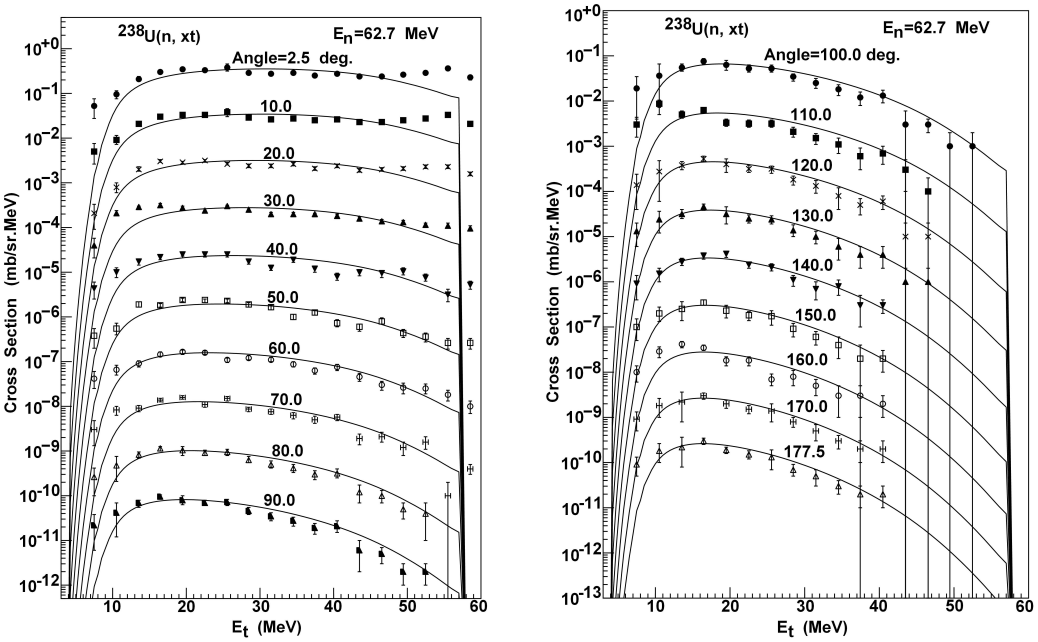

Fig. 13. Calculated triton emission DDXs compared with experimental data [4] at incident energy 62.7 MeV. The data are shifted downward by factors of 10^0, 10^{-1}, 10^{-2}, etc.

Though the experimental data for alpha emission DDXs show some structures, the calculated results at incident energies from 34.5 to 62.7 MeV are in reasonable agreement with experimental data for emission energy above 26.0 MeV. The comparison of calculated results with experimental data at incident neutron energy of 53.5 MeV is given in Fig. 15. The calculated results at incident energy of 96.0 MeV are consistent with experimental data, as shown in Fig. 16, except for the lower emission energy region, where the contribution is mainly from the equilibrium reaction. The description of the alpha emission spectra and DDXs for the low emission energy region is still an open subject in theory and experiment. It can be observed that most LCP emissions occur

in the preequilibrium progress, while for alpha particles, a large component comes from the equilibrium process at low emission energies.

In some cases, the highest emission energy of experimental data is larger than that of the calculated results. Since (n, p), (n, d) and (n, t) reactions are endergonic processes, with $Q_{\rm p}$=-2.82 MeV, $Q_{\rm d}$=-5.40 MeV, and $Q_{\rm t}$=-4.91 MeV, and the (n, α) reaction is an exoergic process with Q_{α}= 8.72 MeV, the highest energy of the emitted particle should be about the incident energy plus Q. Therefore, the calculated results are reasonable. Some of the fluctuations in the experimental data, especially for emission angles above 90°, also need to be checked experimentally.

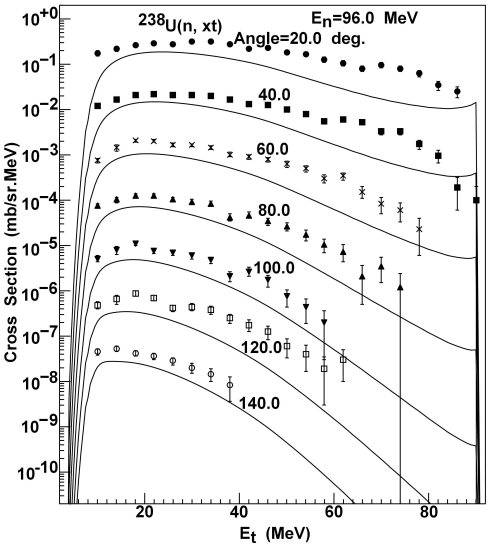

Fig. 14. Calculated triton emission DDXs compared with experimental data [4] at incident energy 96.0 MeV. The data are shifted downward by factors of 10^0, 10^{-1}, 10^{-2}, etc. The experimental data are taken from Ref. [5]

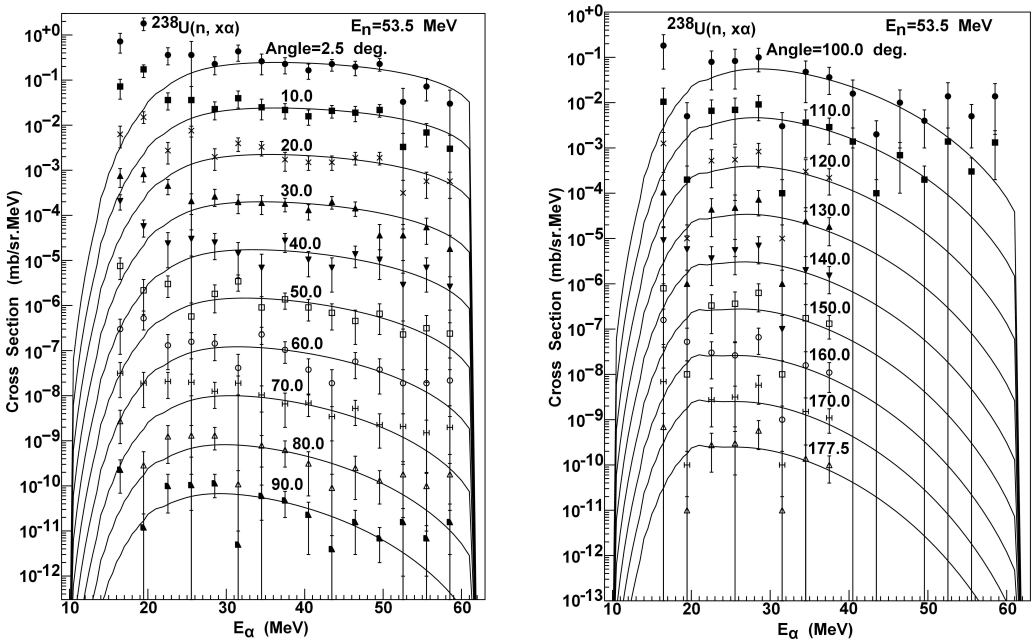

Fig. 15. Calculated alpha emission DDXs compared with experimental data [4] at incident energy 53.5 MeV. The data are shifted downward by factors of 10^0, 10^{-1}, 10^{-2}, etc.

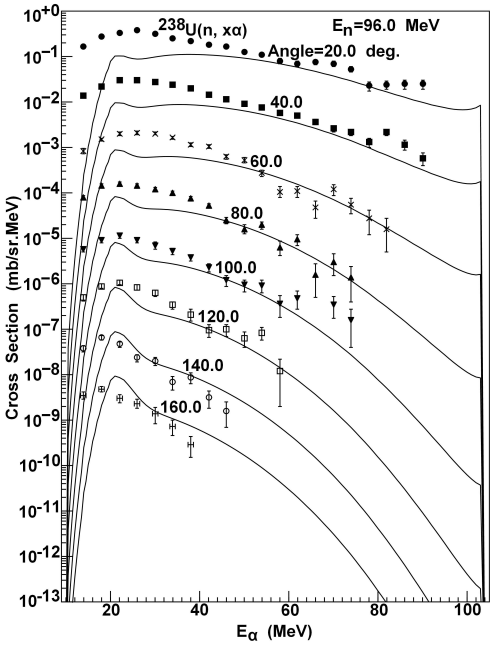

Fig. 16. Calculated alpha emission DDXs compared with experimental data [4] at incident energy 96.0 MeV. The data are shifted downward by factors of 10^0, 10^{-1}, 10^{-2}, etc. The experimental data are taken from Ref. [5]

4 Conclusions

All cross sections, angular distributions, energy spectra and DDXs for the n+^{238}U reaction have been consistently calculated at incident energies below 150 MeV. Good agreement with experimental data is generally obtained. The LCP emissions have been analyzed using the exciton model including the improved Iwamoto-Harada model and the equilibrium-state theories. The theoretical models reproduce the measured energy spectra and DDXs of LCP emissions reasonably well, and give generally better agreement with experimental data than previous analyses. In some cases, the calculated results underestimate the experimental DDXs at low emission energies, where the contribution is mainly from the equilibrium reaction and more investigation is needed. The agreement shows that the exciton model considering the improved Iwamoto-Harada pickup mechanism is reliable for predicting the preequilibrium LCP emissions induced by neutrons on fission nuclei. All of the present results have been transformed to ENDF-formatted files for application.

References

1 R. C. Haight, M. B. Chadwick, and D. J. Vieira, Los Alamos Sci. Mag., **70**: 52 (2006)
2 G. Aliberti, G. Palmiotti, M. Salvatores, and C. Stenberg, Nucl. Sci. Eng., **146**: 13 (2004)
3 A.J. Koning, J.-P. Delaroche, O. Bersillon, Nucl. Instrum. Meth. Phys. Res. A, **414**: 49-67 (1998)
4 E. Raeymackers, S. Benck, I. Slypen, J.P. Meulders, N. Nica, V. Corcalciuc, and A. Koning, Phys. Rev. C, **68**: 024604 (2003)
5 V. Blideanu et al, Phys. Rev. C, **70**: 014607 (2004)
6 J. J. Griffin, Phys. Rev. Lett., **17**: 478 (1966)
7 P. G. Young et al, Comprehensive nuclear model calculations: theory and use of the GNASH Code, Proc. IAEA Workshop Nuclear Reaction Data and Nuclear Reactors-Physics, Design, and Safety, edited by A. Gandini and G. Reffo (Singapore: World Scientific, 1996), p. 227.
8 C. K. Cline, Nucl. Phys. A, **193**: 417 (1972)
9 C. Kalbach, Z. Phys. A, **283**: 401 (1977)
10 C. Kalbach, Phys. Rev. C, **71**: 034606 (2005)
11 M. C. Duijvestijn et al, Annals of Nuclear Energy, **33**: 1196 (2006)
12 I. Ribansky et al, Phys. Lett. B, **45**: 318 (1973)
13 F. Sébille et al, Nucl. Phys. A, **756**: 229 (2005)
14 A. Iwamoto, et al, Phys. Rev. C, **26**: 1821 (1982)
15 J. S. Zhang, et al, Z. Phys. A, **344**: 251 (1993)
16 J. S. Zhang and S. J. Zhou, Chinese Journal of Nuclear Physics, **18**: 28 (1996)
17 Han, Yinlu et al, Phys. Rev. C, **81**: 024616 (2010)
18 Han, Yinlu et al, Phys. Rev. C, **74**: 044615 (2006)
19 Y. L. Xu et al, Int. J. Mod. Phys. E, **24**: 1550005 (2015)
20 X. W. Su and Y. L. Han, Int. J. Mod. Phys. E, **24**: 1550092 (2015)
21 N. Bohr and J. A. Wheeler, Phys. Rev., **56**: 426 (1939)
22 D. L. Hill and J. A. Wheeler, Phys. Rev., **89**: 1102 (1953)
23 C. Kalbach and F. M. Mann, Phys. Rev. C, **23**: 112-123 (1981)
24 C. Kalbach, Phys. Rev. C, **37**: 2350-2370 (1988)
25 F. Tovesson, A. Laptev, T. S. Hill, Nucl. Sci. Eng., **178**: 57 (2014)
26 P.W. Lisowski et al, Nucl. En. Agency Nucl. Data Committee Reports,, **305**: 177 (1991)
27 O. A. Shcherbakov et al, J. Nucl. Sci. Tech., Supplement, **2**: 230 (2002)